Propagation of Material and Manufacturing Uncertainties in Composite Helicopter Rotor Blades

Tobias Pflumm * Willem Rex † Manfred Hajek ‡

Institute of Helicopter Technology
Technical University of Munich, 80333 Munich, Germany

The effects of material and manufacturing uncertainties of a composite UH-60A helicopter rotor blade on the beam properties, the rotating natural frequencies, the aeroelastic response and vibratory loads in hover and in forward flight are studied. The multidisciplinary rotor blade design framework of this study consists of three main components (*DYMORE*, *VABS* and the structural preprocessor *SONATA-CBM*) that are wrapped into the *OpenMDAO* open-source computing platform for system analysis and multidisciplinary optimization. Two separate Monte-Carlo simulations are performed with 1000 samples each. Both material and manufacturing uncertainties propagate through all levels of the simulation, resulting in substantial impacts on natural frequencies, elastic blade tip response and the 4/rev vibratory hubforces.

Nomenclature

CAD	Computer-Aided Design
COV	coefficient of variation
LHS	Latin-Hypercube sampling
MCS	Monte-Carlo simulation
MLE	maximum likelihood estimate
SD	standard deviation
VABS	Variational Asymptotic Beam Sectional Analysis
$(.)_{\parallel}$	parallel to fiber direction
$(.)_{\perp}$	perpendicular to fiber direction
E	Young's modulus
G	shear modulus
m_{00}	mass per unit length
m_{22}	mass moment of inertia about y axis
m_{33}	mass moment of inertia about z axis
X_{m2}	mass center location (y-direction)
X_{m3}	mass center location (z-direction)
k_{ij}	coefficient of the 6x6 stiffness matrix
Ψ	azimuth
ρ	density
θ_3	fiber orientation
T	steady thrust
Q	steady torque
$F_{x,y,z}$	4/rev vibratory hubforces
$M_{x,y,z}$	4/rev vibratory hubmoments

*Graduate Research Assistant, tobias.pflumm@tum.de
†Graduate Research Assistant, willem.rex@tum.de
‡Professor and Department Head, hajek@tum.de

Presented at the 45th European Rotorcraft Forum, Warsaw, Poland, 17-20 September, 2019.

Introduction

The large number of constraints and design drivers from various disciplines makes the helicopter rotor blade development process difficult, time consuming and costly. The entire design process represents a classical aeroelastic problem, where the aerodynamic behavior, the structural elasticity and vibrational dynamics have to be studied simultaneously. The behavior can therefore not be examined with separate analysis of the different disciplines [1]. The integration of all appropriate disciplines in the design process implies not only limitations on the design from various disciplines, but also defining and accounting for interactions so that the disciplines influence design decisions simultaneously rather than sequentially [2]. Historically, the design and development of improved or entirely new rotor blades is conducted by departments in a company that maintain their separate simulation codes for performing their specific tasks [1]. This modular approach narrows the scope of solutions, because each department focuses on individual objectives satisfied by individual design parameters. Mutual interactions can only be covered by numerous iterations. In contrast to that, a multidisciplinary approach offers a more systematic development process that is able to design a better helicopter rotor [2]. Because of the impact, the rotor behavior has on the overall performance of the helicopter and on customer noticeable vibratory characteristics, rotor aeroelastic effects should be considered in the earliest stages of the design process [3].

An additional known problem is that the rotor system behavior can be very sensitive to modification in some parameters and real problems are rarely described by a set of fixed parameters. For example, it has been reported that

the coefficients of variation of the elastic moduli of a composite lamina can be 5 – 15% due to uncertainties associated with fiber and matrix material properties, fiber volume fractions, fiber orientation and undulation, intralaminar voids, etc. [4]. Murugan et. al. [5] showed the effect, such aleatory uncertainties (irreducible uncertainty as it cannot be reduced through modeling techniques) can have to the aeroelastic response of the helicopter rotor and vibratory hub loads. A Monte-Carlo analysis revealed considerable deviations from baseline-predictions, with its extreme value of 600% increase of vibratory hub loads because of resonance conditions. Bernardini et al. showed that the sensitivity of vibratory loads to the design variables for epistemic uncertainty (can be reduced by the increased knowledge or representation of the physics) of the inflow models, can be of such magnitude, that the optimal design of one inflow model performs worse (for some load components, even opposite) than the baseline design when calculated with a different inflow model [6] . Compared to the traditional multidisciplinary rotor blade optimization proposals, Li introduced manufacturing constraints and proposes durability and fatigue analysis in a probabilistic design method to control the impacts of material, shape and load uncertainties on the rotor blade structural performance [7]. By conducting Monte-Carlo simulations, she showed the impacts of geometric perturbation (ply waviness on the inner surface) and material property uncertainties for the aeroelastic behavior and the stress distributions. She combined the Monte-Carlo simulation generating manufacturing and service load uncertainties and the classical structural design method to find a robust solution [8–10]. Li states that the under-representation of uncertainties is a significant reason why the industry is not yet comfortable to use multidisciplinary design optimization methods. The analysis and optimization methods struggle with the performance of predicting the behavior accurately to allow a safe and robust final design. On top of that, current structural rotor blade models are simplified to that extend, that a result of such a design optimization is not precise enough and still has to be refined by manual iterations. Subsequently, the transition to a full 3D CAD description becomes once again a long and iterative task.
The objective of this study is to evaluate the effect of aleatory uncertainty propagation with a high fidelity composite helicopter rotor blade structural model.

Methodology

The multidisciplinary rotor blade design framework used in this study is named *SONATA* (Structural Optimization and Aeroelastic Analysis) [11]. Like most environments it consists of three main components that are managed by *OpenMDAO* [12], an open-source computing platform for multidisciplinary design optimization (MDO) and system analysis, written in Python. This framework addresses two of the most important aspects: low implementation effort and computational efficiency. The first requirement is handled by using few end-user visible concentrated classes in an object-oriented programming paradigm to achieve the desired functionalities during execution. The second requirement is amplified by using high-performance computing resources such as the MPI and PETSc library. [12]

The first component is an aeromechanic analysis of the helicopter rotor, which includes flexible multibody dynamics, nonlinear finite elements and an aerodynamic model that is using the Peters-He dynamic inflow formulation together with 2-D steady airfoil polars. *Dymore* [13] was chosen as tool for both the a dynamic analysis in the time domain as well as a model analysis in the frequency domain. In this context, one-dimensional beam elements are used to describe the rotor blade due to the much simpler mathematical formulation and reduced computational effort compared to a full three-dimensional finite element model of the composite rotor blade [14]. Although, three-dimensional finite element models are the most accurate description of a composite component, it is still not appropriate to use in rotor blade predesign because of the extensive preprocessing and solving effort involved [7]. Typically, this approach decouples the realistic composite blade definition and the manufacturability constraints from the aeromechanic analysis. Thus, problems and inconsistencies in the blade design cannot be discovered until later in the process where changes are costly and time consuming [15]. The slender characteristic of rotor blades allow the simplification to treat them as one-dimensional body. By means of the Variational Asymptotic Beam Sectional Analysis (*VABS*), formulated by Hodges and his coworkers, the behavior that is associated with the reduction of two dimensions can be accurately represented [16]. *VABS* splits the three-dimensional elastic problem of an initially twisted and curved anisotropic rotor blade into a one-dimensional nonlinear beam analysis and a two-dimensional linear cross-section analysis [17]. *VABS* represents the second component of our environment.

A geometric definition of a rotor blade using computer-aided design (CAD) software is straightforward, but the transfer to a meshed cross-sectional representation can prevent automated design optimization. This is one reason why the structural rotor blade models of current methods have often an inaccurate level of detail and miss important stuctural elements and components of the rotor blade (e.g. balance and tuning masses are hardly ever captured). The presented methodology [11] of the third component of the framework, the preprocessor *SONATA-CBM*, incorporates the structurally relevant components and supports a rapid transition to a commercial CAD system by providing an interface, so that the conversion to a full three-dimensional CAD description of the resulting rotor blade design does not become a long and iterative task once again.

Pursuing a common goal as the NASA's Revolutionary Vertical Lift Technology Project (RVLT) to provide validated tools for multidisciplinary design, analysis and optimization (MDAO) of rotorcraft, bringing the three components together to the same programming language ad-

dresses the need for a low implementation effort at user level so they are flexible and easy to use with *OpenMDAO* [18].
The decision to develop Python modules and interfaces was additionally inspired by the idea of a robust multi-fidelity preliminary rotorcraft design method [19] and by NASA's effort to develop a Python module for existing rotorcraft design and analysis tools for the use of *OpenMDAO* referred to as RotorCraft Optimization Tools (*RCOTOOLS*). *RCOTOOLS* currently incorporates interfaces to the NASA Design and Analysis of RotorCraft (*NDARC*) vehicle sizing tool and the Comprehensive Analytical Model of Rotorcraft Aerodynamics and Dynamics II (*CAMRAD II*) [18].

Dymore [13] is used to represent the helicopter rotor and is included into the *OpenMDAO* framework as an *Explicit Component*. This is realized by wrapping the C written code *Dymore* to Python using *SWIG*. More details on the connection between *OpenMDAO* and *Dymore* are described in [20]. In general the *Dymore* library provides multiple functions for communication with other Python modules of which only a subset is used in this work. These functions are depicted in figure 1. *get*- and *set*-functions are

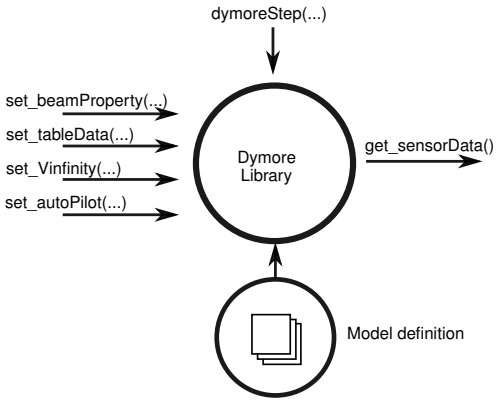

Fig. 1: *Dymroe* interface integrated into *OpenMDAO*

used to write values to the model and read data from the model. In particular, beam properties, the flight velocity and auto pilot characteristics can be updated in the model during execution. In addition, the function *set_tableData(...)* can be used to modify all model properties which are represented by a table in *Dymore*, like the rotor angular velocity, actuator displacement, etc. The name of the corresponding table is an argument of the function. Likewise, sensor states can be observed during exection and the values are returned to *OpenMDAO* as *numpy*-array. The sensor has to be defined in the model definition and the name of the sensor is again passed as function argument. Using the function *dymoreStep(...)* the calculation in time domain as well as in frequency domain in controlled from *OpenMDAO*. This function allows to select the time step width for each step individually. In this work the functions are used to run multiple fan plot analysis, hover and forward flight simulations in parallel. Similarly, *SONATA-CBM* has been developed with the use of *pythonOCC*, an *Opencascade* CAD-Kernel wrapper for python [21].

Description of the UH-60A Rotor Model

A rotor model similar to the UH-60A main rotor is used in the analysis herein. The structure of the rotor model, established in *Dymore* is represented by a multibody formulation. The rotor blades and the rotor shaft are represented by finite beam elements. Except for the pitch links and the servos that include lengthwise stiffnesses, the control linkage and the rotor hub are represented by rigid bodies. The nonlinear characteristic of the lag-damper is included as well. Aerodynamic collocation points are distributed along the radial span and 2-D steady airfoil polars depending on Mach number are used to represent the rotor blade aerodynamic forces and section pitch moment. The *Peters-He* model, which is already integrated in *Dymore* is used to account for the inflow dynamics. The rotor model is described in detail in ref. [20]. In this work, the rotor is operated in a wind tunnel setup. Which means that the fuselage, empennage and tail rotor are not included into the simulation framework. However, the rotor can be trimmed towards free flight conditions [20]. The considered flight states are a low speed horizontal forward flight corresponding to the airloads flight test counter C8513 [22] and a symmetric hover case at the altitude and blade loading of the airloads counter C8513 shown in table 1. The rotor model with baseline rotor blade structural properties is validated against these flight conditions and additional flight states in ref. [20].

Flight States	hover	low speed flight (C8513)
advance ratio, μ	0.0	0.149
C_W/σ	0.0792	0.0792
rotor speed, N_r, [RPM]	258	258
density, ρ, [kg/m^3]	1.13	1.13

Table 1: Considered flight states

Rotor Blade Structural Analysis

The *SONATA* rotor blade is defined in the blade reference coordinate system which is denoted x_r, y_r and z_r in figure 2. In the case of the generic UH-60A rotor blade of figure 3, its origin is located at the center of rotation and is rotating with the blade. x_r is pointing along the blade axis from root to tip; y_r is pointing towards the leading edge. Together with x_r and y_r, z_r it describes a right-handed coordinate system in 3D space.

The wireframe that defines the outer shape of the rotor blade is defined by a collection of airfoils that are projected along x_r, after translating them to the non-dimensional pitch-axis location, rotating them about the twist angle around x_r, scaling them to the desired chord length and moving them onto the blade reference curve. Because both the rotor blade reference curve and the beam reference curve can be arbitrarily curved and twisted, secondary local coordinate systems (CBM frames) are defined for each

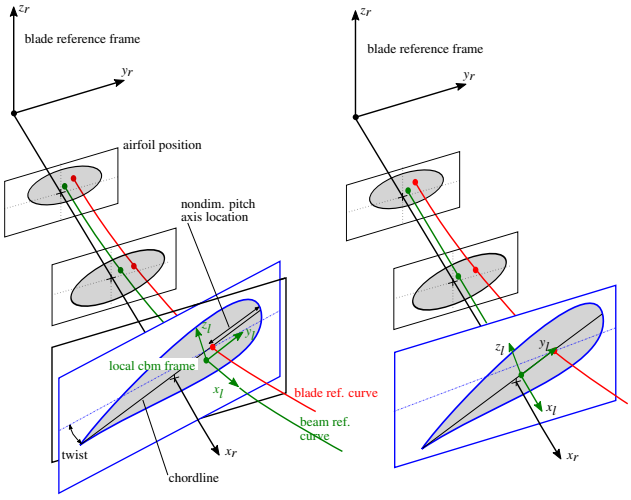

a) general SONATA blade definition with arbitrary reference curve

b) beam ref. curve is parallel to x_r of the blade reference frame

Fig. 2: SONATA blade and beam definition

structural two-dimensional composite cross-section that is modeled. The structural mass and stiffness properties of the beam are defined with respect to the local CBM-frame. The unit vector of the local CBM frame x_l must be tangent to the beam reference curve. The unit-vectors y_l and z_l are in the plane normal to the beam reference curve with y_l pointing towards the leading edge. In figure 3 the

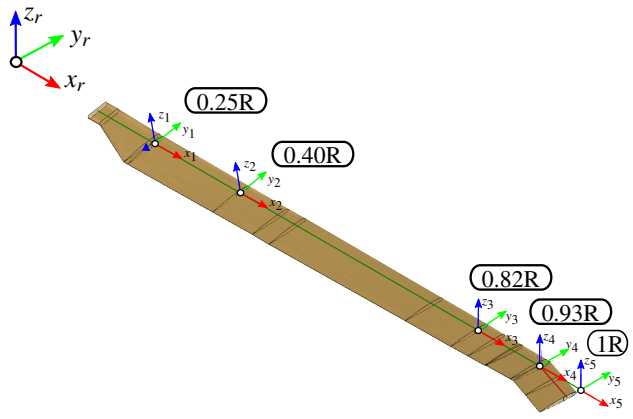

Fig. 3: Outer shape of the UH-60A blade, generated from the dataset of Davis [23]. Specific cross-sections are distributed at $0.25R$**,** $0.40R$**,** $0.82R$**,** $0.93R$ **and** $1R$**.**

outer surface of the generic UH-60a rotor-blade is illustrated showing five discrete radial location, at which the inner composite-structure is modeled with a two-dimensional finite element discretization. Subsequently at each cross-section the beam sectional properties are calculated with *VABS* and are passed to the beam definition of the dymore rotor-blade. In this particular case the beam reference curve is parallel to x_r of the blade reference frame, so that the cross-sections are parallel to the y_r-z_r plane. The blade attachment and root is not specified in the context of this study. Yet to provide a complete description of the blade, the structural mass and stiffness properties of the original UH-60A are used up to the first cross-section at $0.25R$.

The SONATA structural preprocessor [11] has been developed with the intention to reproduce the composite rotor blade manufacturing procedure during the process of topology generation. Starting with an arbitrary outer closed curve, the layers are placed on top of each other in a consecutive manner. This assists to avoid complex constraints during an optimization and to ensure manufacturability and a solution within proper bounds. Each layer has an assigned material with start and end coordinates, a thickness and fiber orientation. Every parameter or groups of such can serve as design variables in an optimization. After the layup process on top of the outer boundary curve is finished, webs are introduced and subsequently new closed geometries are generated, at which the layup procedure can be repeated. Remaining cavities can be filled with core materials and additional trim masses can be inserted. At this point each layer has bottom and top sets of B-Splines. Succeeding the topology generation, the discretization procedure follows the topology generation in a reversed direction with respect to the layup-definition, starting from the innermost layers and moving outwards. Each layer is meshed by an orthogonal projection of distributed nodes from the top B-Splines set onto the bottom set. Detected corners are distinguished by their style and refined afterwards. Based on the two-dimensional mesh the VABS input file is generated. VABS carries out the constitutive modeling to recover beam stiffness and inertia properties. If internal loads are assigned three-dimensional displacement, strain and stress fields can be recovered within the cross-section [24].

In figure 4 the structural cross-section of $0.4R$ is shown. The architecture of this cross-section is representative for all other four sections. The rotor-blade has a 1mm thick skin of four layers e-glass with both $0°$ and $\pm 45°$ fiber orientation. A nickel erosion protection strip of 0.82mm thickness protects the leading edge of the blade against rain and sand. While the blade skin its $\pm 45°$ layers serves mechanically for the transfer of torsional forces, the spar inside the cross-section is responsible for the transfer of the centrifugal loads and allowing a defined flapping and lagging movement. For this study a design was chosen that combines a distinctive c-spar of unidirectional high-tensile strength (HT) carbon in the leading edge region with a box spar. The c-spar was chosen to provide the possibility to embed an additional trim mass into the structure and move the mass center closer the pitch-axis. The box-spar was chosen to provide a great flexibility for the mechanical properties of the design. The material was chosen to be an intermediate modulus carbon fiber epoxy composite with a fiber volume content (FVC) of 60%. The layup was therefore set to provide 4 layers of different fiber orientations in all major directions [0°, 45°, −45°, 90°] with baseline thicknesses of [1.35mm, 1.35mm, 1.35mm, 0.5mm]. The cavity in the rear part of the cross-section is filled with a HexWeb 5.2-1/4-25 aluminum honeycomb

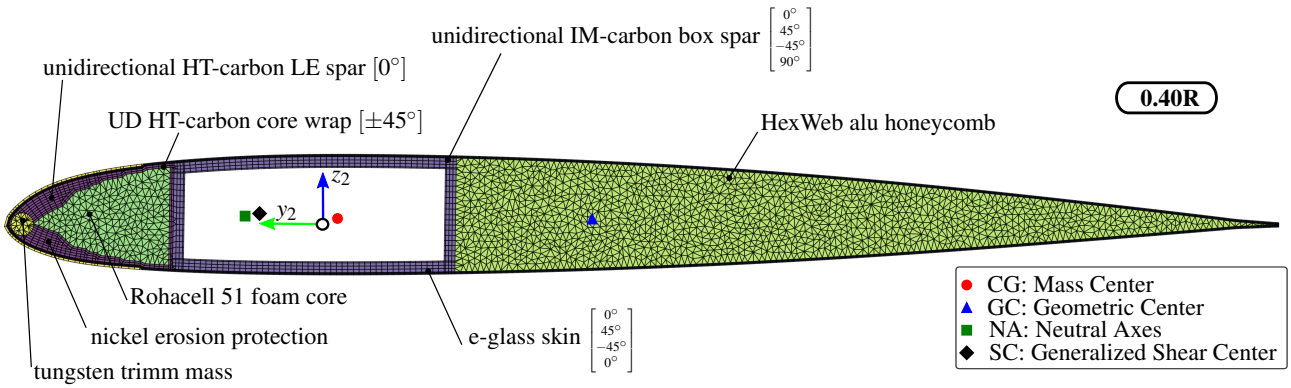

Fig. 4: Composite rotor-blade cross-section at 0.4R

material [25] and the front part is filled with a Rohacell IG-F 51 foam. The structurally integrated front cavity is used to place tuning masses into the structure by replacing the rohacell foam core with a tungsten-epoxy granulate at radial station 0.25R and 0.93R to make sure that the eigenfrequencies of the rotor do not cross multiples of the rotor-harmonic at nominal rotational speed and that the rearward mass of the swept tip is balanced. The only other difference of the other sections compared to the illustration of figure 4 (SC-1095), besides small changes in chord-length, is the airfoil-shape SC-1094R8 between 0.5R and 0.82R.

In figure 5 and figure 6 the stiffness and mass properties of the described rotor blades are shown. They are baseline values for the Monte-Carlo Simulation (MCS) and are compared against the original UH-60A properties from Davis [23]. To provide a complete description of the beam they are joined with reference properties up to 0.25R.

The peaks in the mass per unit length m_{00} indicate the location of the tuning masses at 0.25R and 0.93R. The same applies to the center of mass location in chordwise direction X_{m2}, moving the center of mass towards the leading edge. The large gradient at the end of the mass-properties can be explained by the swept blade tip, which moves the cross-section backward relative to the beam reference coordinate system. While, mass distribution and center of gravity location are relatively similar to the reference UH-60A properties, the new composite design drastically reduces the mass moment of inertia about the y-axis.

The symmetric 6x6 sectional stiffness matrix, (1-extension, 2,3-shear, 4-twist, 5,6-bending) relates the sectional axial strain ε_1, transverse shearing strains ε_2 and ε_3, twisting curvatures κ_1 and two bending curvatures κ_2 and κ_3 to the axial force F_1, transverse shear forces F_2 and F_3, twisting moment M_1 and two bending moments M_2 and M_3. [24]

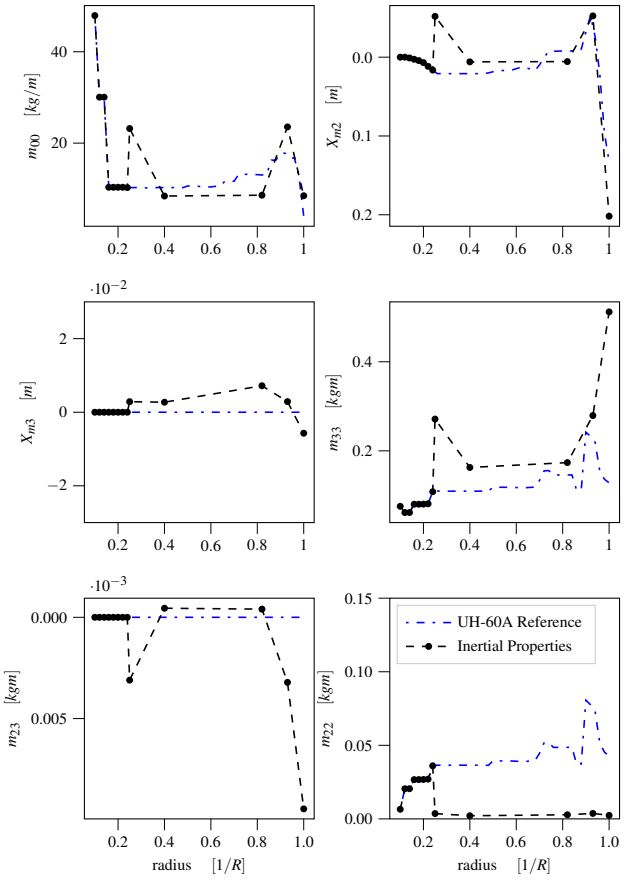

Fig. 5: Baseline Beam Inertial Properties

$$\begin{pmatrix} F_1 \\ F_2 \\ F_3 \\ M_1 \\ M_2 \\ M_3 \end{pmatrix} = \begin{pmatrix} \underline{k_{11}} & k_{12} & k_{13} & k_{14} & k_{15} & k_{16} \\ k_{12} & \underline{k_{22}} & k_{23} & k_{24} & k_{25} & k_{26} \\ k_{13} & k_{23} & \underline{k_{33}} & k_{34} & k_{35} & k_{36} \\ k_{14} & k_{24} & k_{34} & \underline{k_{44}} & k_{45} & k_{46} \\ k_{15} & k_{25} & k_{35} & k_{45} & \underline{k_{55}} & k_{56} \\ k_{16} & k_{26} & k_{36} & k_{46} & k_{56} & \underline{k_{66}} \end{pmatrix} \cdot \begin{pmatrix} \varepsilon_1 \\ \varepsilon_2 \\ \varepsilon_3 \\ \kappa_1 \\ \kappa_2 \\ \kappa_3 \end{pmatrix}$$

In figure 6 the diagonals of the stiffness matrix are illustrated. The axial stiffness k_{11} The torsional stiffness k_{44}, flap-stiffness k_{55} and lag-stiffness k_{66} are all increased compared to the UH-60A reference blade. The peak stiffnesses of k_{44} and k_{66} at the tip are a result of the offset from the reference axis. The fan diagram in figure 7

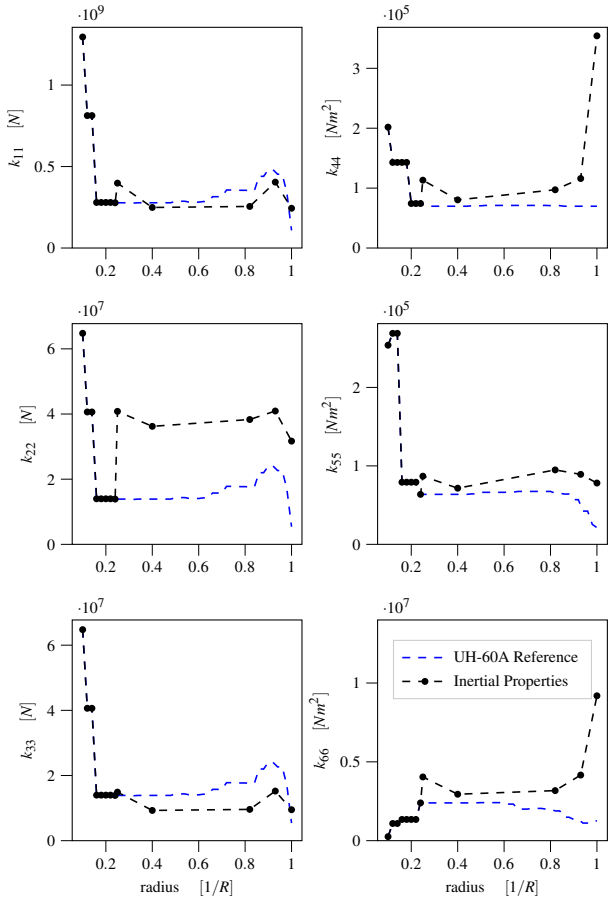

Fig. 6: Baseline Beam Stiffness Properties

shows the corresponding eigenfrequencies of the rotor versus rotational speed. For the modal analysis no aerodynamic forces were considered, the pitchlinks and the rotor-controls were also assumed to be rigid. The fundamental lag (1st mode), the first three flap (2nd, 3rd, 6th)and the torsional (4th mode) frequency are relatively similar to the original UH-60A. Particularly the fourth flap frequency (4th mode) is increased due to the higher stiffnesses.

Monte-Carlo Simulation

The objective of this study is to evaluate the effect of aleatory material and manufacturing uncertainties, and how they affect the overall helicopter rotor behavior. A Monte-Carlo approach is chosen for this study (highlighted in figure 8). In the first analysis the material uncertainties are studied. Studies have shown that the mechanical properties of composites show a considerable variance due to uncertainties associated with fiber and matrix material properties, fiber volume fractions, fiber orientation and undulation, intralaminar voids, etc. [4]. The baseline elastic properties ot the fiber composite materials of the rotor-blade are derived from a semi-empiric Puck approach [27] using basic reference values for HT- and IM-carbon fiber and epoxy matrix material with a fiber volume content (FVC) of 60%. The unidirectional HT-carbon composite is used for the c-spar (in the following referred as "material 1"). The unidi-

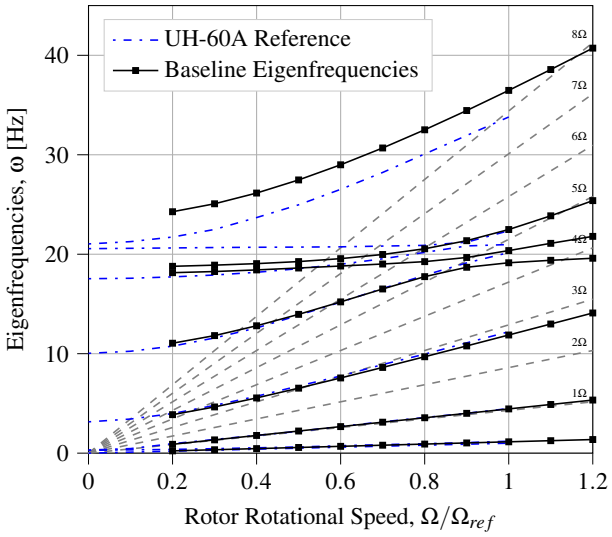

Fig. 7: Baseline Rotor Fan Diagram, Reference UH-60A data obtained from ref. [26]

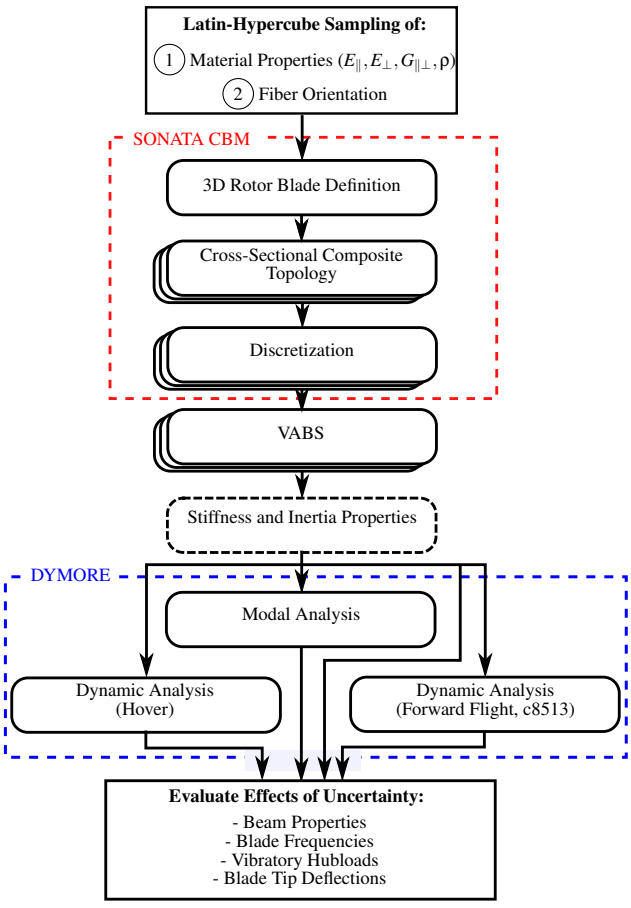

Fig. 8: Monte-Carlo Simulation Procedure

rectional IM-carbon composite is used for the box-spar (in the following referred as "material 3"). Latin-Hypercube sampling (LHS) is used to generate a near-random normal distribution of material-properties $E_\parallel, E_\perp, G_{\parallel\perp}$ and ρ. The mean (μ) and the coefficient of variation (COV) of the material properties are listed in table 2. The COV is the nor-

malized measure of dispersion of a probability distribution. It is defined as the ratio of the standard deviation (SD, σ) to the mean of the distribution. Similar to ref. [5], the COVs

Material properties	Mean	COV
$E_{1\parallel}$	139.36 GPa	7 %
$E_{1\perp}$	12.62 GPa	4 %
$G_{1\parallel\perp}$	5.89 GPa	12 %
ρ_1	1.536 g/cm^3	5 %
$E_{3\parallel}$	177.76 GPa	7 %
$E_{3\perp}$	12.62 GPa	4 %
$G_{3\parallel\perp}$	5.89 GPa	12 %
ρ_3	1.572 g/cm^3	5 %

Table 2: Uncertainties in material properties taken from [4] based on a COV of 5% in microlevel composite properties.

assumed in this study are taken from reference [4]. Onkar et. al. describe the effect of a COV of 5% in microlevel composite properties such as elastic properties of the fiber E_f, ν_f and matrix phase E_m, ν_m and FVC, changing the macrolevel effective material properties for different composite systems. The COV in $E_{\parallel}$ was found to be approximately 7% for all types of composite systems, whereas the shear-modulus $G_{\parallel\perp}$ showed a larger variation of 12%. The material density is herein assumed to be normally distributed with a COV of 5% for this study. Drawing 1000 random samples from the distribution, figure 9 shows the statistical distribution of the material 3 properties. The maximum likelihood estimation shows standard deviations close to the prescribed COVs for both materials.

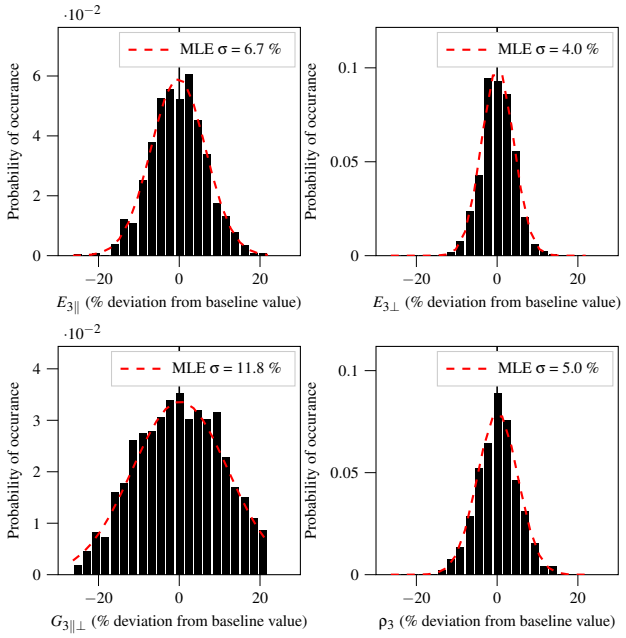

Fig. 9: Probability distribution of properties of the IM-carbon composite (material 3)

In the second analysis of this study the uncertainties in fiber orientation θ_3 of the four box spar layers is studied. Until now, the rotor-blade manufacturing process is still hand layup and a distortion of ply layup angles is possible during the manufacturing process. For this separate analysis a SD of 5 degree is assumed. Table 3 shows the design variables. Equal to the first study, 1000 LHS samples are generated for the Monte-Carlo Simulation.

Fiber orientation	Mean	SD
$\theta_{3,bs1}$	0 °	5 °
$\theta_{3,bs2}$	45 °	5 °
$\theta_{3,bs3}$	-45 °	5 °
$\theta_{3,bs4}$	90 °	5 °

Table 3: Uncertainties in fiber orientation

After a sample is drawn from the distribution, the rotor blade structural analysis is performed including the cross-section topology generation (described in figure 3), followed by the discretization and calculation of stiffness and inertia properties with *VABS*. The resulting beam-properties are evaluated together with the results from the modal, hover and forward flight analysis.

Results and Discussion

This section is divided into separate analysis. To study the material and manufacturing uncertainties separately allows to gain a better insight into the mechanisms and the propagation of uncertainties to the rotor's dynamic behavior.

Propagation of Material Uncertainties

Beam Properties The resulting cross-sectional beam property distribution of the material uncertainty Monte-Carlo Simulation are discussed. To demonstrate the sufficiency of the number of samples the convergence of SD of torsional- (k_{44}) and flap (k_{55}) stiffness at radial station 0.4R are shown in figure 10.

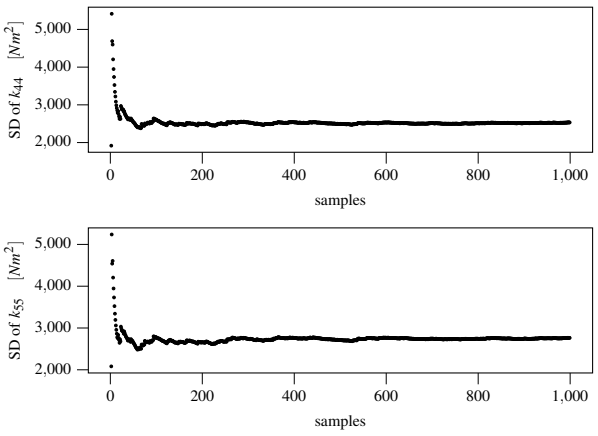

Fig. 10: Convergence of the SD of torsional- k_{44} and flap stiffness k_{55} for the material uncertainty analysis

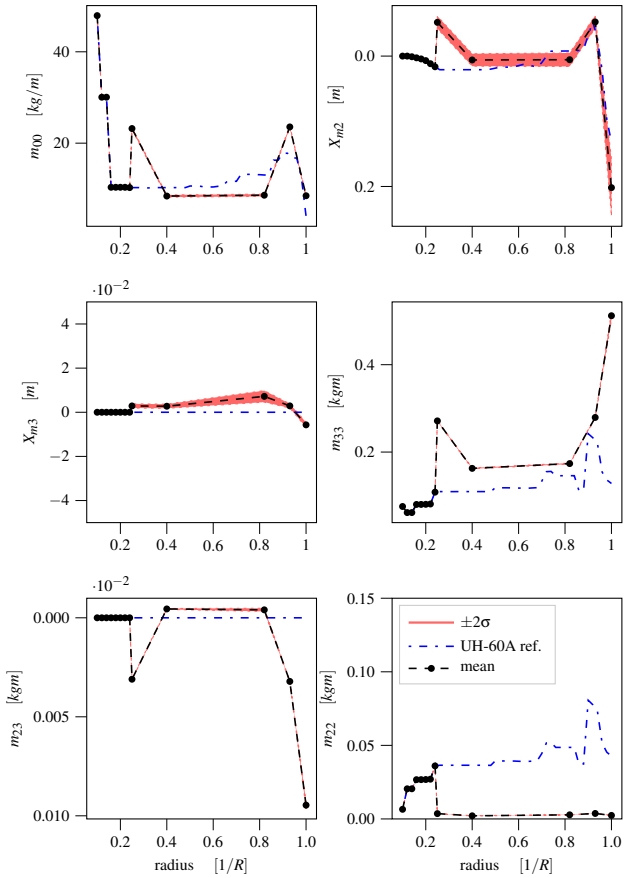

Fig. 11: Beam Inertial Properties and $\pm 2\sigma$ confidence interval for the material uncertainty analysis

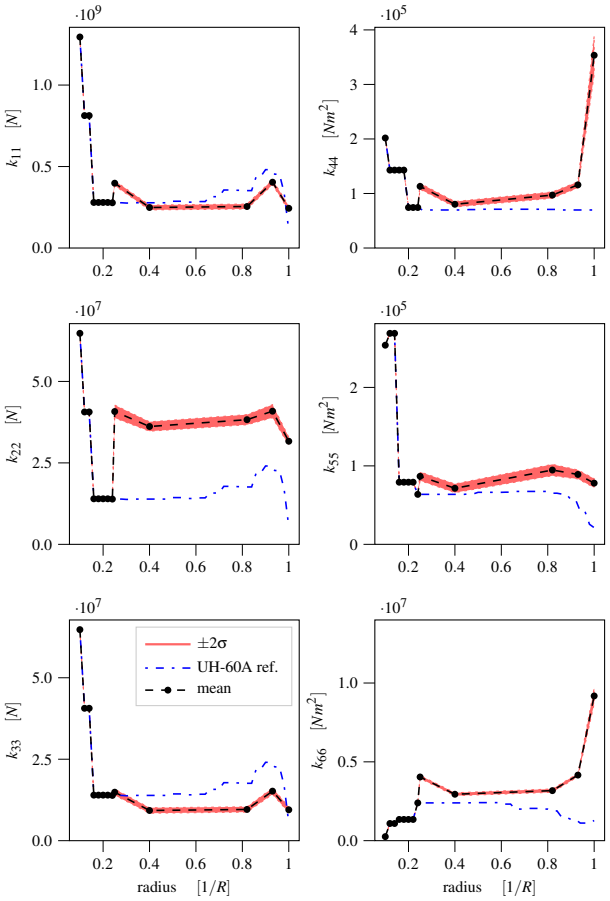

Fig. 12: Beam Stiffness Properties and $\pm 2\sigma$ confidence interval for the material uncertainty analysis

In figure 11 and figure 12 the mean inertial properties and diagonals of the stiffness matrix are shown together with a $\pm 2\sigma$ confidence interval showing the variance of the different entries. The largest influence of uncertainty exists for the center of gravity in chordwise direction X_{m2} with a COV of 10.2% at 0.25R, while the mass per unit span m_{00} is only affected with a COV of 1.4%. The mass moment of inertia m_{22} (COV of 2.1%) and m_{33} (COV of 0.3%) are also just slightly influenced.

The axial, torsional, and flap stiffness show COVs of 3.0, 3.2 and 3.9% at 0.4R, respectively. The lag stiffness k_{66} shows the lowest impact by the introduced uncertainties with a COV of 1.6%. Figure 18 shows the histogram of the classical 4x4 stiffness matrix for radial station 0.4R. Note that for the Gaussian distributed input, most of the results are also represented by a Gaussian normal distribution. It is shown that in particular the torsional coupling relations k_{14}, k_{45}, k_{45} of this cross-section are barely influenced by the added uncertainty. At the same time the flap-lag coupling relation k_{56} shows the largest sensitivity with a COV of 8.2%.

All five cross-sections of this blade have the same layout, therefore not only the properties along the span stay relatively constant, but also the influence of uncertainties. However, when comparing the histograms of 0.4R (figure 18) and 1R (figure 19), it is noticed that the torsional coupling terms become much more sensitive at the swept blade tip, increasing the COV from $< 1\%$ to $\approx 5\%$.

In the next sections, it will be discussed how the scatter in resulting mass and stiffness properties changes the dynamic response of the rotor.

Natural Frequencies In this section the effect of material uncertainties on the rotating natural frequencies of the rotor is evaluated. The placement of natural frequencies of the rotor is an important design aspect to reduce the dynamic loads at the rotorhub and propagation of vibration into the fuselage. A well tuned rotor will also help to reduce fatigue of components in the rotating frame. Usually, this is done by the targeted introduction of additional tuning masses into the structure (as it was done for this rotor blade) in such a way that the natural frequencies are a safe distance away from the rotor harmonics. A rule of thumb states that distance to be approximately 0.2/rev [28]. A rotor particularly transfers the frequencies that are integer multiples of the number of blades and their neighbors from the rotating to the fixed frame. In this case, for a four bladed rotor the frequencies at 3Ω, 4Ω and 5Ω as well as 7Ω, 8Ω and 9Ω are important to keep a save distance from.

Again, to demonstrate the sufficiency of the samples-size, the convergence of the SD of the second and the fourth flap frequency are shown at nominal rotor speed in figure 13.

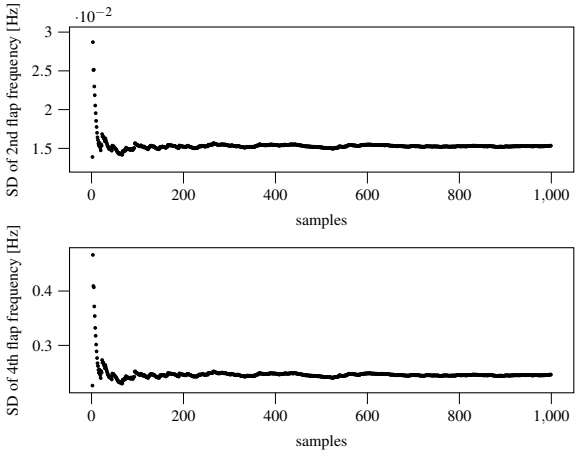

Fig. 13: Convergence of the SD of second and forth flap frequencies at nominal rotational speed for the material uncertainty analysis 1)

In figure 14 the mean rotating natural frequencies are shown from 20% to 120% rotor rotational speed together with a $\pm 2\sigma$ confidence interval. Because the UH-60A rotor has a distinctive flap and lag elastomeric hinge, the first two frequencies represent the rigid body lag and flap modes. The impact of uncertainty varies with each mode. Higher modes are affected to a larger extend because the structural elasticity becomes dominant compared to the effect of centrifugal stiffening at the lower modes. This is also the reason why the 7th mode (4th flap mode) shows a larger influence at lower rotational speeds.
In the next sections, it is discussed how the dispersion in eigenfrequencies affect the dynamic response and the 4/rev vibratory hubloads of the rotor.

Hover The symmetric hover flight state is studied. The uncertainty of the elastic tip deflections can give an indication for the probability and the magnitude of miss-alignment that would need to be counteracted by a blade tracking procedure. Note however, that the 4 blades of the rotor are identical for this study and no blade dissimilarity is considered.
In figure 15 the histograms of the elastic flap, lag and torsion response in hover are shown. The response is the relative measure of the tip to the blade attachment and is not superimposed with the flap, lag and torsion response of the elastomeric bearing. The flap, lag and torsion response distributions have a COV of 6.2%, 5.6% and 3.9% respectively.

Forward Flight In this section the blade tip response (flap, lag and torsion) is evaluated over azimuth position

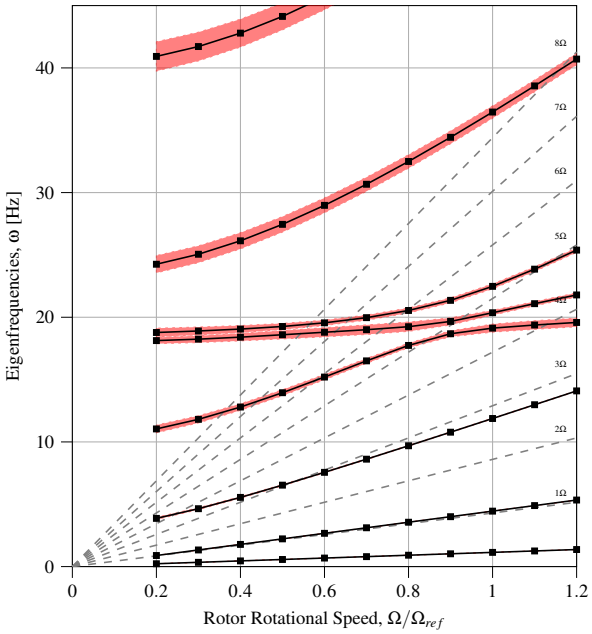

Fig. 14: Mean eigenfrequencies with $\pm 2\sigma$ confidence interval versus rotational speed for the material uncertainty analysis

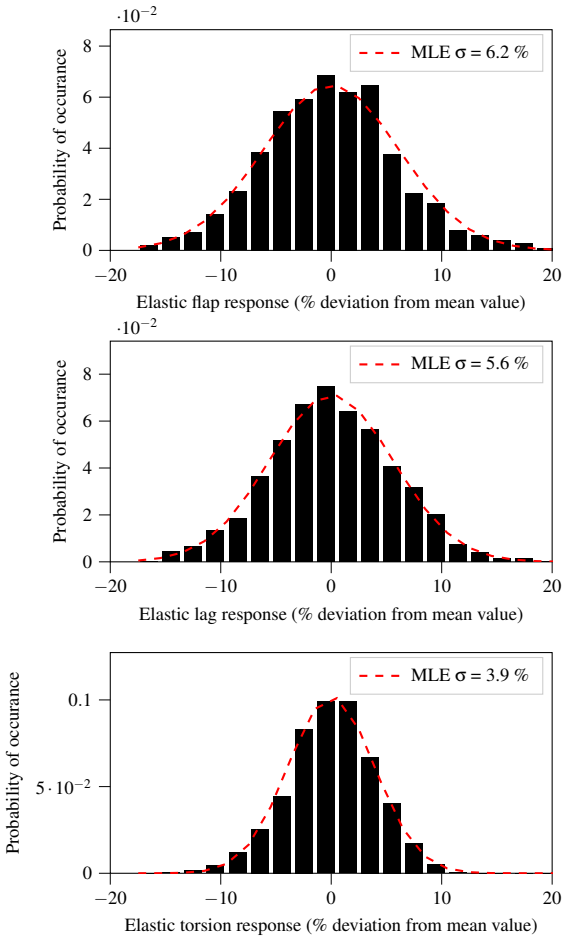

Fig. 15: Histograms of the elastic flap, lag and torsion response in hover for the material uncertainty analysis

for the forward flight state. Additionally, the 4/rev vibratory hub forces and hub moments are studied.
The flight state considered for this study is a low speed horizontal forward flight corresponding to the airloads flight test counter 8513 [22] listed in table 1 with a advance ration of $\mu \approx 0.15$ and a blade loading of $C_w/\sigma = 0.0792$.
Because *Dymore* performs a time-domain simulation and does not assume periodicity, the steady state periodic response of the rotor is extracted by simulating approximately 13 rotor revolutions, evaluating the variance of the last two revolutions and joining them to form a periodic response.

Similar to the elastic blade tip response in hover, its behavior is studied during the forward flight state, shown in figure 16. However in this case, the blade tip response varies along the azimuth position of the blade. The mean values and the $\pm 2\sigma$ confidence interval are shown. The amplitudes of the torsion response shows a deviation of approximately 0.5 degree. The uncertainty of amplitude in the 5/rev periodic response of the torsional response, will potentially have also an impact on the hub vibration levels. The flap response is less than the observed torsional response. As mentioned before, the rotor particularly transfers the frequencies that are integer multiples of the number of blades and their neighbors from the rotating to the fixed frame, so that frequencies of 3Ω, 4Ω and 5Ω will transform to 4/rev frequencies in the fixed frame. In figure 17 the effect onto the the 4/rev vibratory hubloads is evaluated. The six components are the longitudinal shear (F_x), lateral shear (F_y) and vertical force (F_z) as well as rolling moment (M_x), pitching moment (M_y) and torque (M_z). These components are obtained by performing a fast Fourier transform (FFT) of the time signal. The 4/rev forces are normalized by the rotor steady thrust (T). The 4/rev moments are normalized by the rotor steady torque (Q). The first interesting observation is that the histogram does not show a Gaussian normal distributions. The second observation is that the F_x, F_y and M_y show the larges deviation with a COV of 24, 18.7 and 19.6% respectively. The vertical components show a COV of 10% while the rolling moment M_x has the smallest COV of 7.1%.

Propagation of Manufacturing Uncertainties

Following the first analysis of material uncertainties, this section evaluates the effects of fiber orientation uncertainties based on the LHS Monte-Carlo simulation with 1000 random samples.

Beam Properties Unlike the first analysis, the parameters of this MCS do not affect the mass or inertial properties of the blade in any way. In figure 22 the mean stiffness together with the $\pm 2\sigma$ confidence interval are illustrated once again. The diagonals of the beam stiffness properties show the effect of fiber orientation is in the same magnitude as the effect of material uncertainty with a COV of 2.8, 4.1, 4.1 and 0.4% for the k_{11}, k_{44}, k_{55} and k_{66} respectively. The coupling relations of the cross-section at 0.4R in figure 20 and 1R in figure 21 demonstrate the substantial effect to the twist-axial k_{14}, twist-flap k_{45}, twist-lag k_{46} coupling relations is noticed. Compared to the material uncertainty study, those terms are increased from a COV <1% to a COV of approximately 30% at 0.4R. At the same time, the effect to lag-stiffness k_{66}, and flap-lag coupling relation k_{56} is relatively small.
The uncertainty in fiber orientation will disturb the symmetric layup of the box-spar that enhances those coupling relations. This effect is amplified at radial station 1R because of the coordinate-system's location.

Natural Frequencies In this section the effect of fiber orientation uncertainties on the rotating natural frequencies of the rotor are discussed. In figure 23 the mean rotating natural frequencies are illustrated together with a $\pm 2\sigma$ confidence interval. The mean torsional frequency (4th mode) is slightly lower compared to the baseline case and the analysis of material uncertainties. The beam properties anticipated that the $\pm 2\sigma$ confidence interval of the torsional mode will also be larger. Note that the -2σ boundary of this mode is very close to the 4/rev rotor harmonic. This shift of torsional frequencies towards the 4/rev is expected to affect the dynamic behavior and the resulting vibratory hubforces and moments adversely.
Similar to the first analysis, the impact of uncertainty varies with each mode. Generally, higher modes are affected to a larger extend because the ratio of structural elasticity and centrifugal stiffening increases.

Hover For the symmetric hover flight state, the fiber orientation uncertainty has the consequence that both the flap and torsion response are affected substantially. Figure 22 shows for this purpose the histogram of the elastic flap, lag and torsion response. The response is the relative tip displacement measure to the blade attachment. The flap response has a COV of 61.6%, the torsion response has a COV of 63.5% while the lag response stays relatively uninfluenced.

Forward Flight The elastic tip response during forward flight is also shown for fiber orientation uncertainty in figure 25. Compared to the tip response of the study of material uncertainty, the torsional response of this analysis shows larger mean amplitudes. The most significant impact is the large $\pm 2\sigma$ confidence interval that has a magnitude of around 5 degree for the torsional response. Note that for all responses, the higher harmonic fraction of the signal becomes much more visible.
Figure 26 shows the 4/rev vibratory hubforces and moments in forward-flight. The increased vibratory loads were anticipated from the previous evaluations. Again, non Gaussian distributions results from the introduced uncertainty. All fractions of the vibratory hubloads show an in-

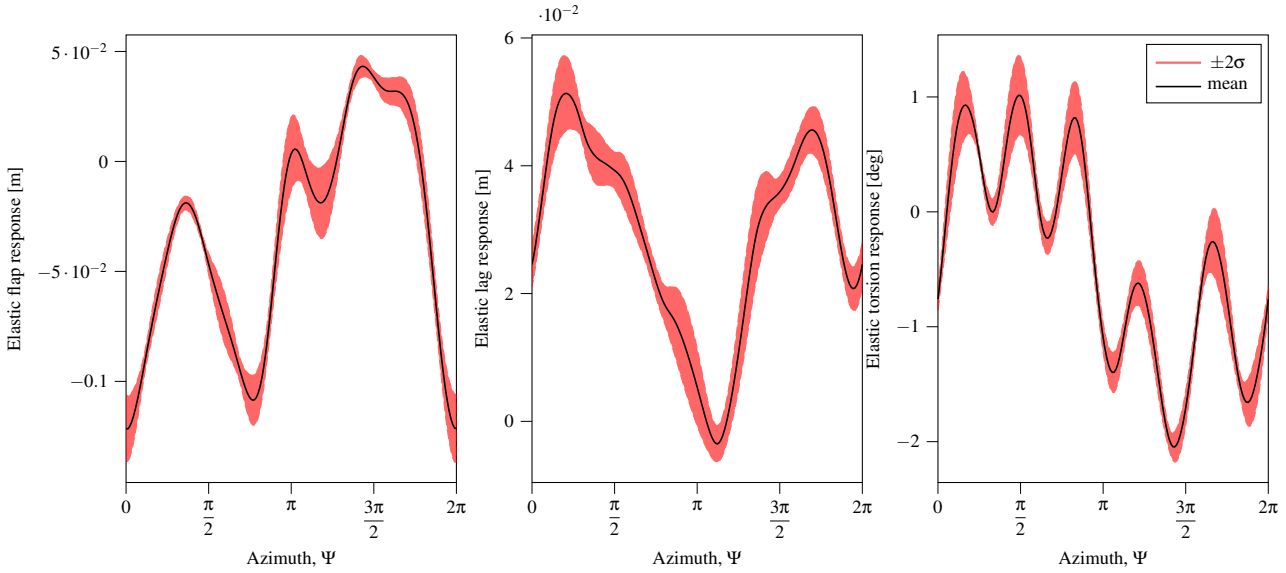

Fig. 16: Elastic flap, lag and torsion response in forward flight with $\pm 2\sigma$ confidence interval for the material uncertainty analysis

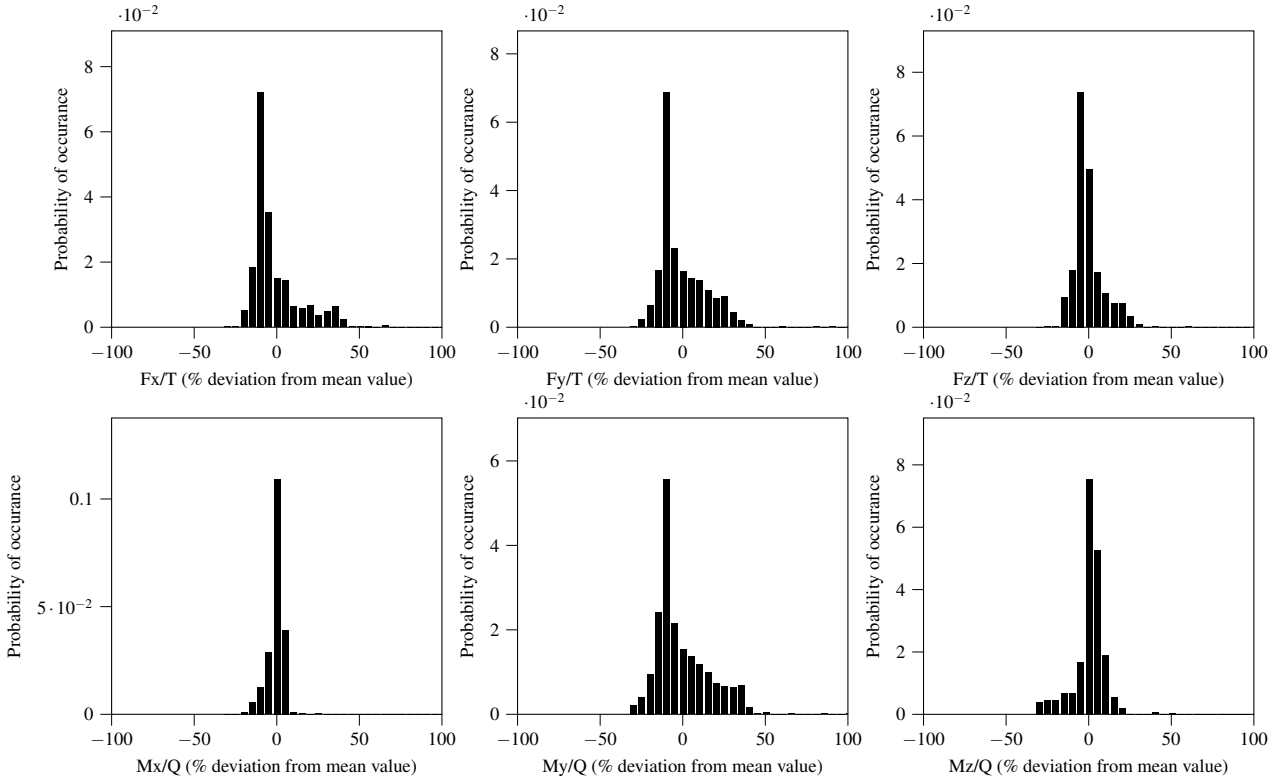

Fig. 17: Histogram of 4/rev vibratory hubforces and moments in forward flight for the material uncertainty analysis

creased distribution. The largest variation is registered at the vertical force and torque components with a COV of 80% and peak values up to 400%.

Conclusions

The effects of material and manufacturing uncertainties of a composite UH-60A helicopter rotor blades on the beam properties, the rotating natural frequencies, the aeroelastic response, and vibratory loads in hover and forward flight are studied. The composite material properties of the rotor

blade spar are considered to be Gaussian distributed. The manufacturing uncertainties are considered by varying the fiber orientations of the box-spar of the rotor-blade. Two separate Monte-Carlo simulations are performed with 1000 samples each. The following conclusions are drawn from this study:

1. The Gaussian distributed uncertainties introduced to the rotor blade result in Gaussian distributed beam properties.
2. The impact of uncertainty to the rotating natural frequencies varies with each mode. Generally, higher modes are affected to a larger extend because the ratio of structural elasticity and centrifugal stiffening increases.
3. The standard deviation of the fiber orientation distribution is assumed to be 5 degree, resulting in a substantial impact on torsional coupling relations that propagate to a large effect on natural frequencies, elastic tip displacement in hover and forward flight and high vibratory hubloads with a COV of 80% with peak values of approximately 400%. The assumption of 5 degrees SD is high and not representative for real uncertainties during the manufacturing process of rotor blades, but shows the significance of this parameter. The change of the fiber orientation of the box-spar layers results in an asymmetric layup is therefore responsible for the large coupling relations.
4. The uncertainties of material properties are derived from a micro-mechanic approach and are more representative of an actual distribution.
5. The assumption of this study is that one sample from the material or fiber orientation is applied to the all five cross-sections with the same value. Hence the material properties and fiber orientation are constant over the span of the rotor blade. In reality however, some parameters presumably vary along the span of the blade and therefore the effects might counteract each other to some extend and change the effect on the rotor blade properties and dynamic behavior.
6. Similar to the issue above, all four rotor-blades are assumed to be equal for each sampled case. No blade dissimilarity is assumed for this study. In reality, blade dissimilarity is counteracted to some extend by a tracking and balancing the blades of a rotor. In the future blade dissimilarity could be investigated with its effect to rotor behavior and tracking and balancing efforts.
7. While aleatory uncertainties have been studied in this work, epistemic uncertainties have not been studied. However it was shown that aeroelastic behavior and especially the vibratory loads can be very sensitive to aerodynamic models. In the future, multi-fidelity studies should be performed to quantify the uncertainty of different aerodynamic models.

The above conclusion show that the uncertainties in composite rotor blades have a considerable effect to the dynamic behavior and the vibratory hubloads and needs to be considered in a multidisciplinary design and optimization methodology of rotor-blades to increase the robustness of the designs.

Acknowledgment

This work is supported by the German Federal Ministry for Economic Affairs and Energy through the German Aviation Research Program LuFo V-2 and the Austrian Research Promotion Agency through the Austrian Research Program TAKE OFF in the project VARI-SPEED. The author would like to thank Simon Beer for contributing to this work during his term project.

Supported by:

Federal Ministry for Economic Affairs and Energy

on the basis of a decision by the German Bundestag

FFG Austrian Research Promotion Agency

References

[1]Tarzanin, F. and Young, D., "Boeing rotorcraft experience with rotor design and optimization," *7th AIAA/USAF/NASA/ISSMO Symp. Multidiscip. Anal. Optim.*, American Institute of Aeronautics and Astronautics, Reston, Virigina, sep 1998.

[2]Adelman, H. M. and Mantay, W. R., "Integrated Multidisciplinary Optimization of Rotorcraft: A Plan for Development," Tech. rep., NASA, 1989.

[3]Rohl, P. J., Kumar, D., Dorman, P., Sutton, M., and Cesnik, C. E. S., "A Composite Rotor Blade Structural Design Environment for Aeromechanical Assessments in Conceptual and Preliminary Design," *American Helicopter Society 68th Annual Forum*, American Helicopter Society, 2012.

[4]Onkar, A., Upadhyay, C., and Yadav, D., "Stochastic finite element buckling analysis of laminated plates with circular cutout under uniaxial compression," *Journal of applied mechanics*, Vol. 74, No. 4, 2007, pp. 798–809.

[5]Murugan, S., Ganguli, R., and Harursampath, D. K., "Stochastic Aeroelastic Analysis of Composite Helicopter Rotor," *Journal of the American Helicopter Society*, Vol. 56, No. 1, jan 2011, pp. 12001–1200113.

[6]Bernardini, G., Piccione, E., Anobile, A., Serafini, J., and Gennaretti, M., "Optimal Design and Acoustic Assessment of Low-Vibration Rotor Blades," *International Journal of Rotating Machinery*, Vol. 2016, 2016, pp. 1–17.

[7]Li, L., *Structural Design of Composite Rotor Blades with Consideration of Manufacturability, Durability, and Manufacturing Uncertainties*, phdthesis, Georgia Institute of Technology, Aug. 2008.

[8]Li, L., Volovoi, V., and Hodges, D., "Probabilistic Design Optimization of Composite Rotor Blades," *49th AIAA/ASME/ASCE/AHS/ASC Structures, Structural Dynamics, and Materials Conference; 16th AIAA/ASME/AHS Adaptive Structures Conference;*, American Institute of Aeronautics and Astronautics, apr 2008.

[9]Li, L., Volovoi, V. V., and Hodges, D. H., "Cross-Sectional Design of Composite Rotor Blades," *American Helicopter Society 63rd Annual Forum*, 2007.

[10]Li, L., Volovoi, V. V., and Hodges, D. H., "Cross-sectional Design of Composite Rotor Blades Considering Manufacturing Constraints," *American Helicopter Society 63rd Annual Forum*, American Helicopter Society, 5 2007.

[11]Pflumm, T., Garre, W., and Hajek, M., "A Preprocessor for Parametric Composite Rotor Blade Cross-Sections," *44th European Rotorcraft Forum, Delft, The Netherlands*, September 2018.

[12]Gray, J. S., Hwang, J. T., Martins, J. R. R. A., Moore, K. T., and Naylor, B. A., "OpenMDAO: An Open-Source Framework for Multidisciplinary Design, Analysis, and Optimization," *Structural and Multidisciplinary Optimization*, Vol. 59, 2019, pp. 1075–1104.

[13]Bauchau, O. A., Bottasso, C. L., and Nikishkov, Y. G., "Modeling Rotorcraft Dynamics With Finite Element Multibody Procedures," *Mathematical and Computer Modelling*, Vol. 33, No. 10-11, 5 2001, pp. 1113–1137.

[14]Datta, A. and Johnson, W., "Three-Dimensional Finite Element Formulation and Scalable Domain Decomposition for High-Fidelity Rotor Dynamic Analysis," *Journal of the American Helicopter Society*, 2011.

[15]Rohl, P., Dorman, P., Sutton, M., Kumar, D., and Cesnik, C., "A Multidisciplinary Design Environment for Composite Rotor Blades," *53rd AIAA/ASME/ASCE/AHS/ASC Structures, Structural Dynamics and Materials Conference*, No. April, American Institute of Aeronautics and Astronautics (AIAA), Reston, Virigina, apr 2012, pp. 1–15.

[16]Cesnik, C. E. S. and Hodges, D. H., "VABS: A New Concept for Composite Rotor Blade Cross-Sectional Modeling," *American Helicopter Society 51st Annual Forum*, 1995.

[17]Cesnik, C. E., Hodges, D. H., and Sutyrin, V. G., "Cross-sectional analysis of composite beams including large initial twist and curvature effects," *AIAA journal*, Vol. 34, No. 9, 1996, pp. 1913–1920.

[18]Meyn, L., "Rotorcraft Optimization Tools: Incorporating Rotorcraft Design Codes into Multi-Disciplinary Design, Analysis, and Optimization," *AHS Specialists Conference on Aeromechanics Design for Transformative Vertical Flight*, AHS, San Francisco, California, jan 2018.

[19]Wirth, D. and Hajek, M., "Probabilistic Methodology for Multi-Fidelity Model-Based Robust Preliminary Design of Rotorcraft," *American Helicopter Society 3rd Annual Forum*, 2017.

[20]Rex, W., Pflumm, T., and Hajek, M., "UH-60A Rotor and Coupled Rotor-Fuselage Simulation Framework Validation and Analysis," *45th European Rotorcraft Forum, Warsaw, Poland*, 2019.

[21]Paviot, T., "pythonOCC, 3D CAD/CAE/PLM development framework for the Python programming language, http://www.pythonocc.org/," .

[22]Bousman, W. G. and Kufeld, R. M., "UH-60A Airloads Catalog," 2015.

[23]Davis, S. J., "Predesign Study For a Modern 4-Bladed Rotor for the RSRA," Tech. Rep. 16155, NASA, March 1981.

[24]Yu, W., Volovoi, V., Hodges, D. H., and Hong, X., "Validation of the variational asymptotic beam sectional analysis," *AIAA Journal*, Vol. 40, No. 10, jan 2002, pp. 2105–2112.

[25]Schwingshackl, C., Aglietti, G., and Cunningham, P., "Determination of honeycomb material properties: existing theories and an alternative dynamic approach," *Journal of Aerospace Engineering*, Vol. 19, No. 3, 2006, pp. 177–183.

[26]Bowen-Davies, G. M., *Performance and Loads of Variable Top Speed Rotorcraft at High Advance Ratios*, Ph.D. thesis, University of Maryland, 2015.

[27]Schürmann, H., *Konstruieren mit Faser-Kunststoff-Verbunden*, Springer, 2005.

[28]van der Wall, B. G., *Grundlagen der Hubschrauber-Aerodynamik*, Springer, 2015.

Appendix:

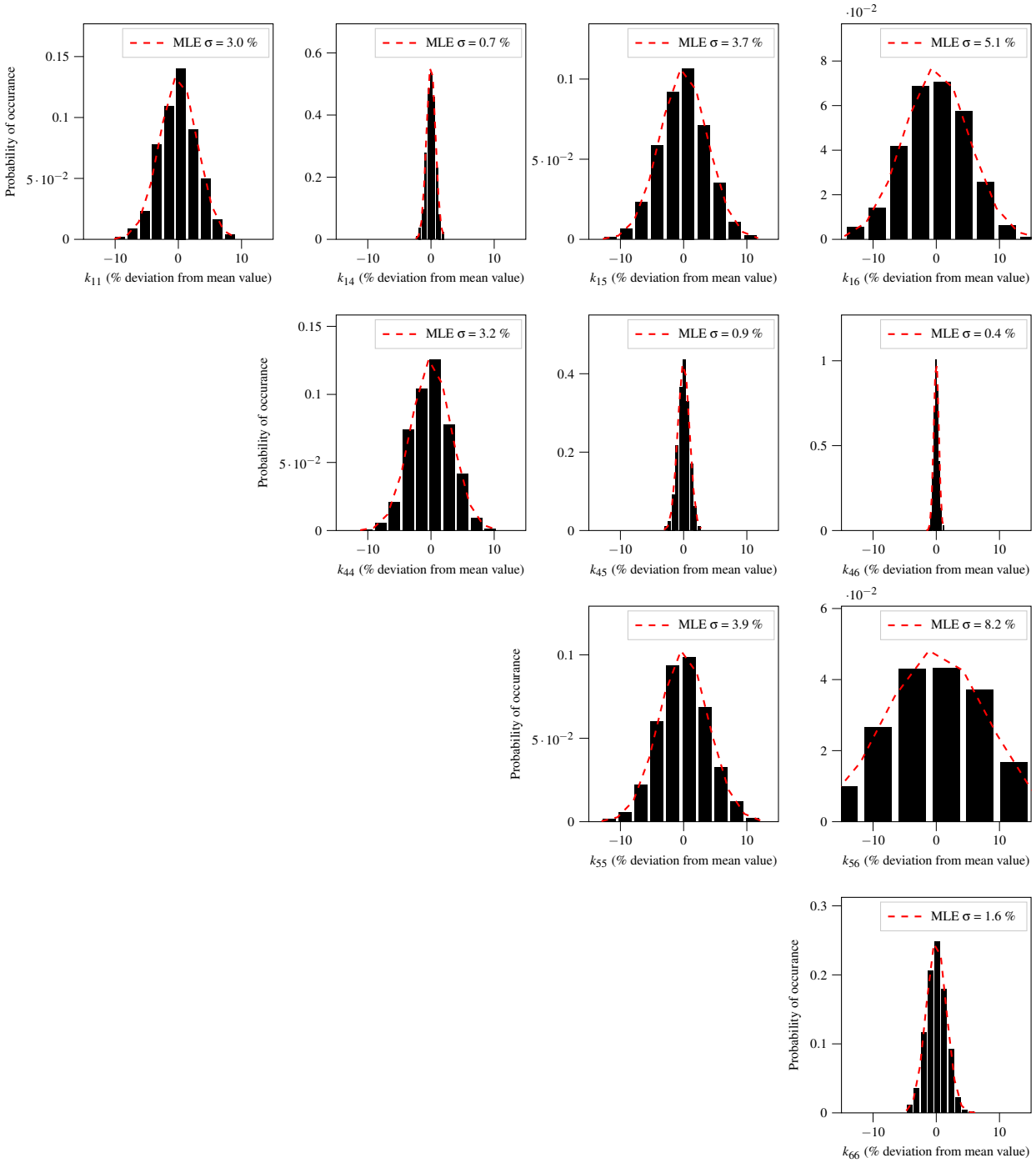

Fig. 18: Histogram of the classical stiffness matrix at 0.4R (material uncertainty analysis)

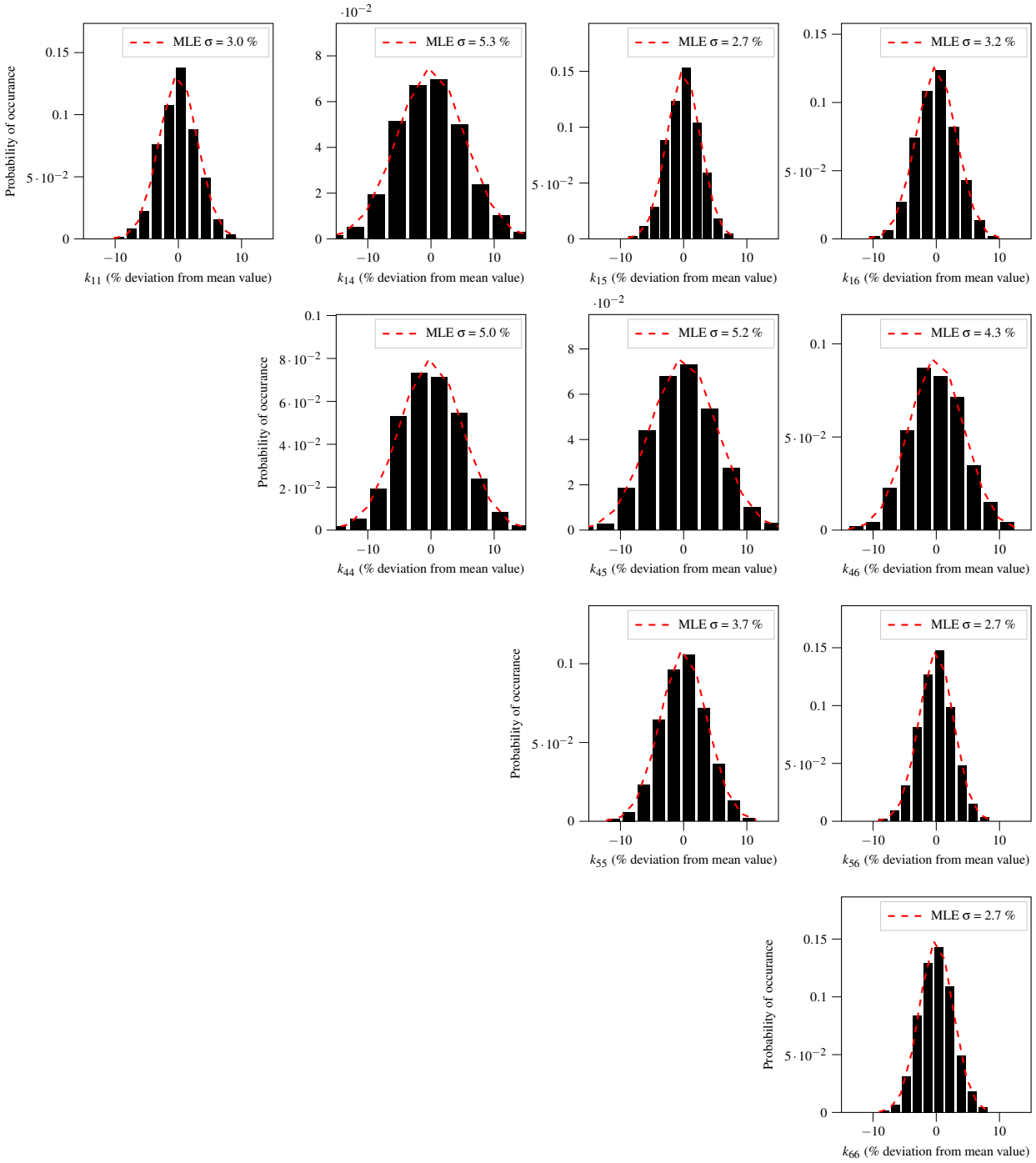

Fig. 19: Histogram of the classical stiffness matrix at 1R (material uncertainty analysis)

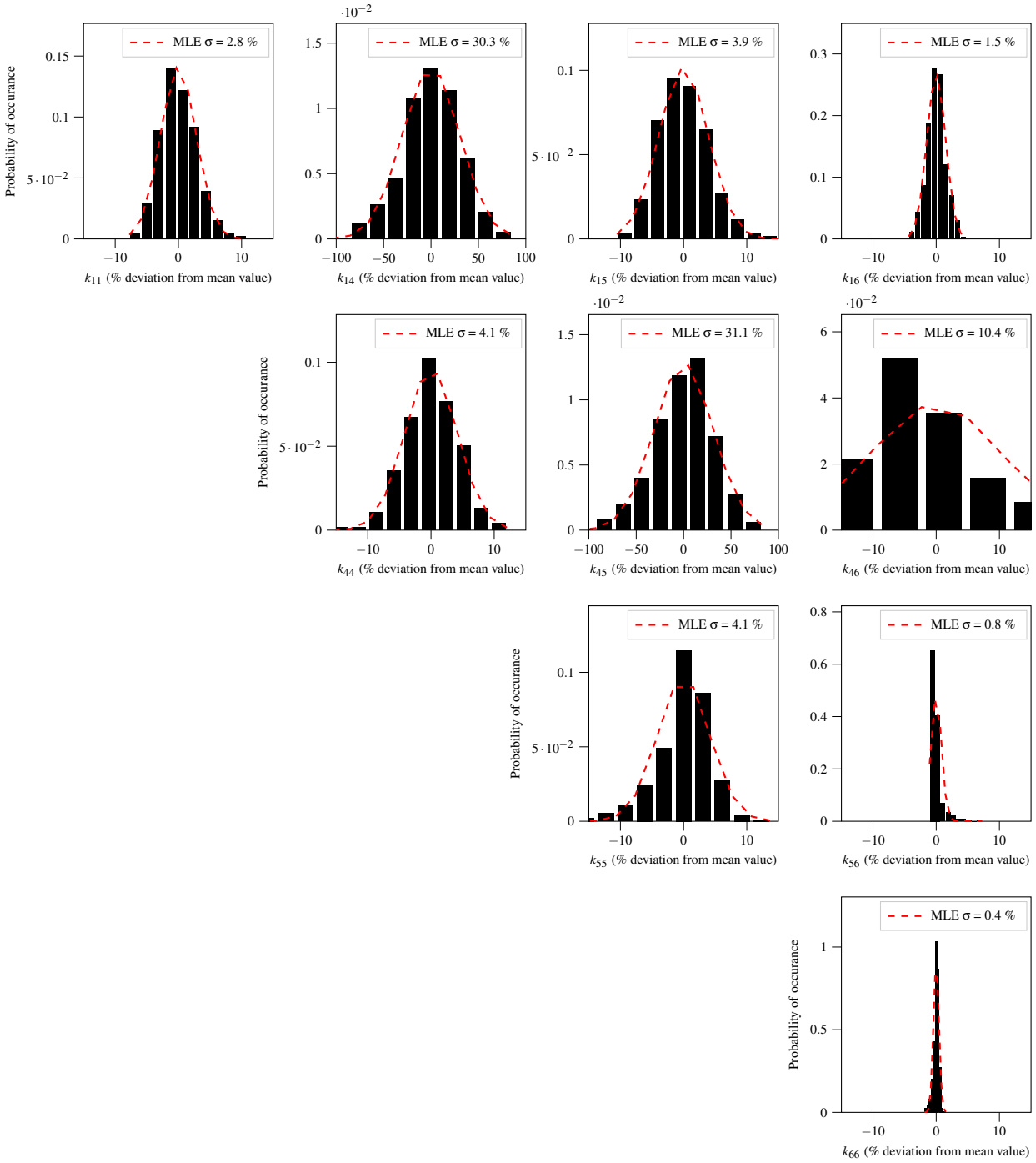

Fig. 20: Histogram of the classical stiffness matrix at 0.4R (fiber orientation uncertainty analysis)

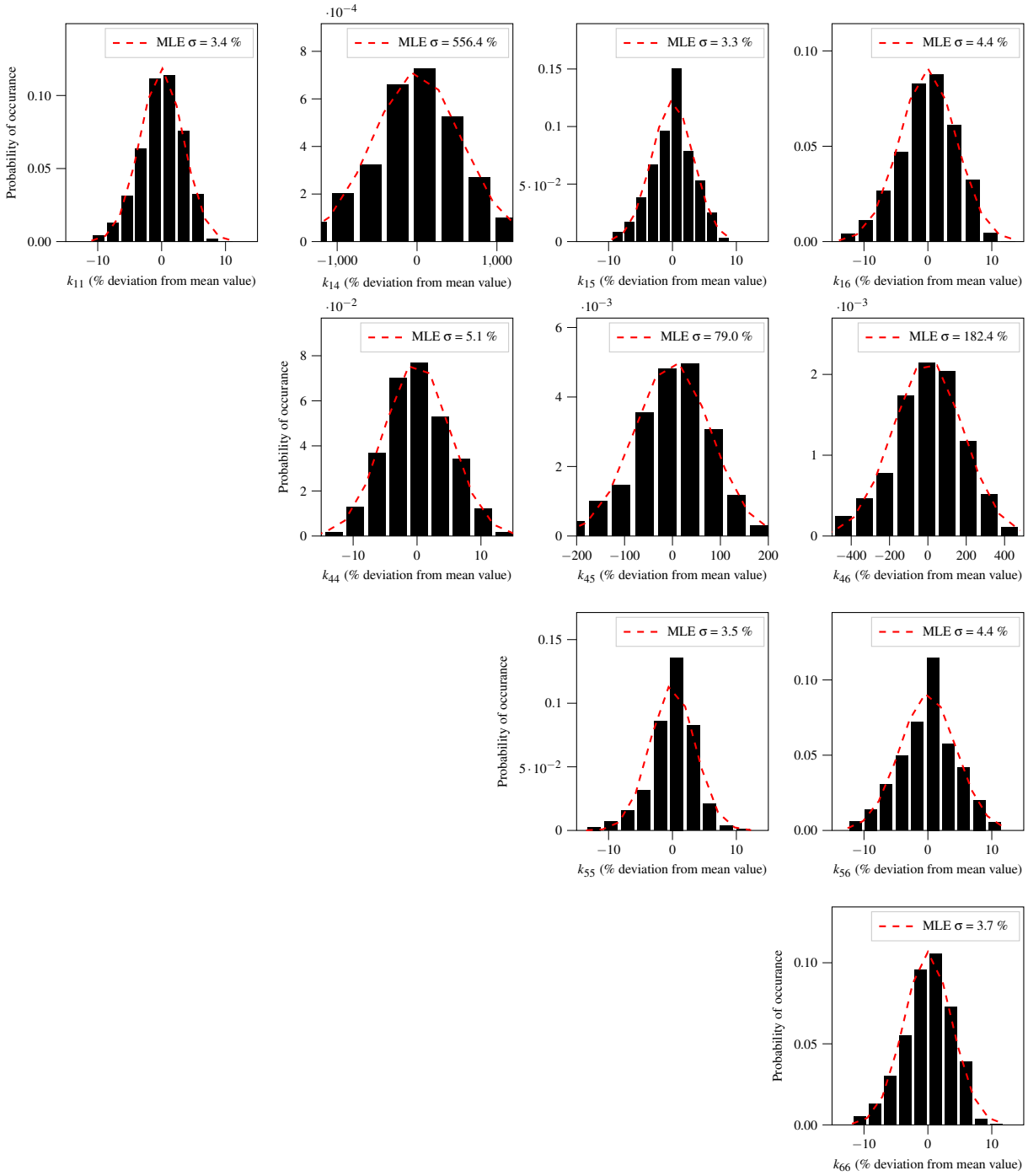

Fig. 21: Histogram of the classical stiffness matrix at 1R (fiber orientation uncertainty analysis)

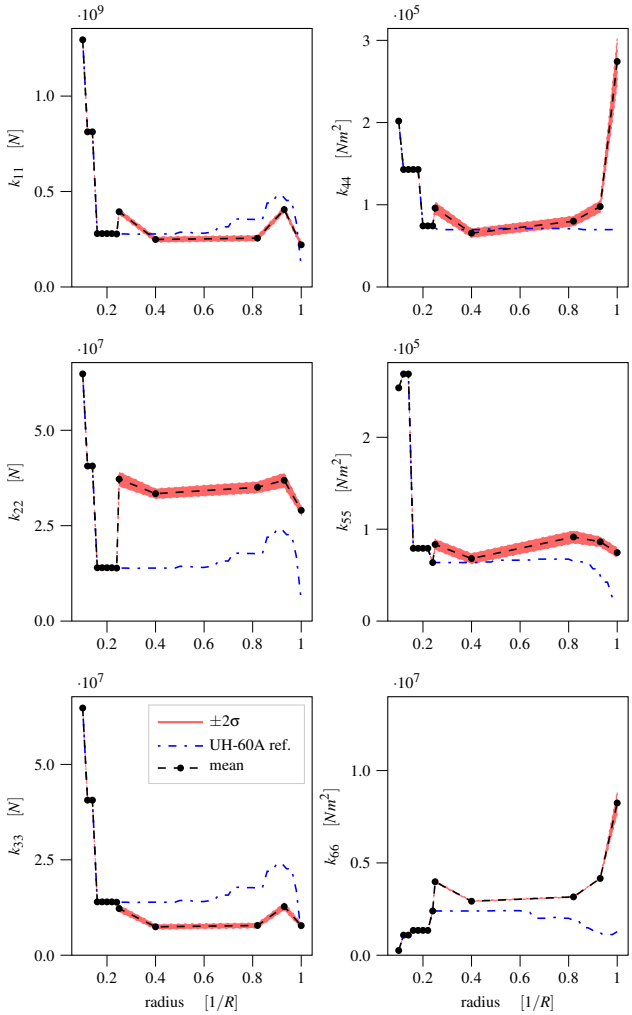

Fig. 22: Beam stiffness properties and ±2σ confidence interval (fiber orientation uncertainty analysis)

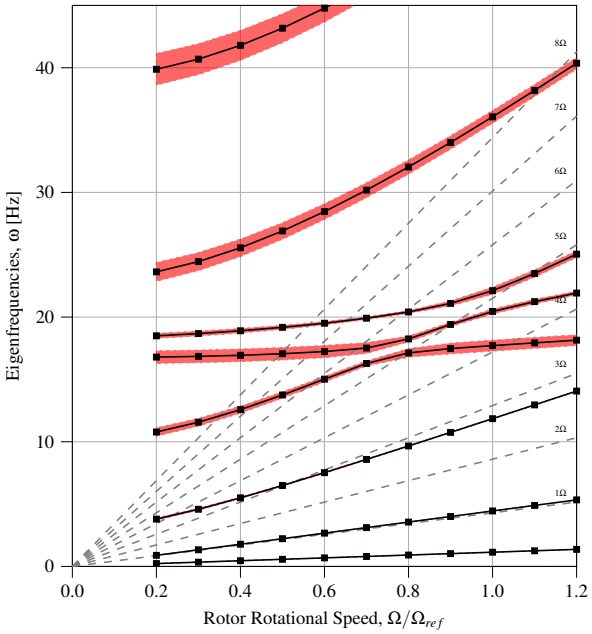

Fig. 23: Mean natural frequencies with ±2σ confidence interval versus rotational speed (fiber orientation uncertainty analysis)

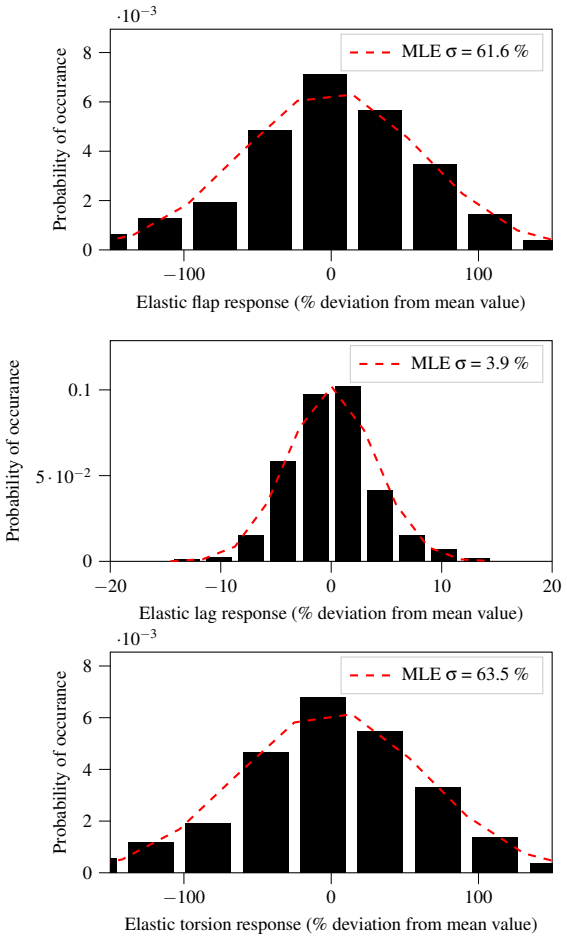

Fig. 24: Histograms of the elastic flap, lag and torsion response in hover (fiber orientation uncertainty analysis)

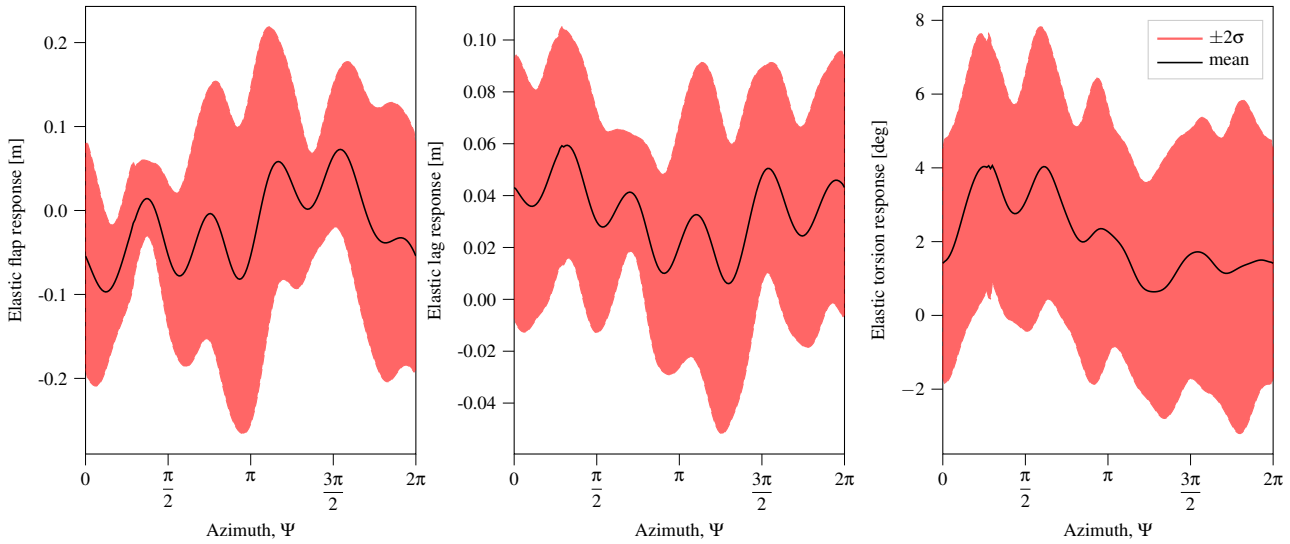

Fig. 25: Elastic flap, lag and torsion response in forward flight with $\pm 2\sigma$ confidence interval (fiber orientation uncertainty analysis)

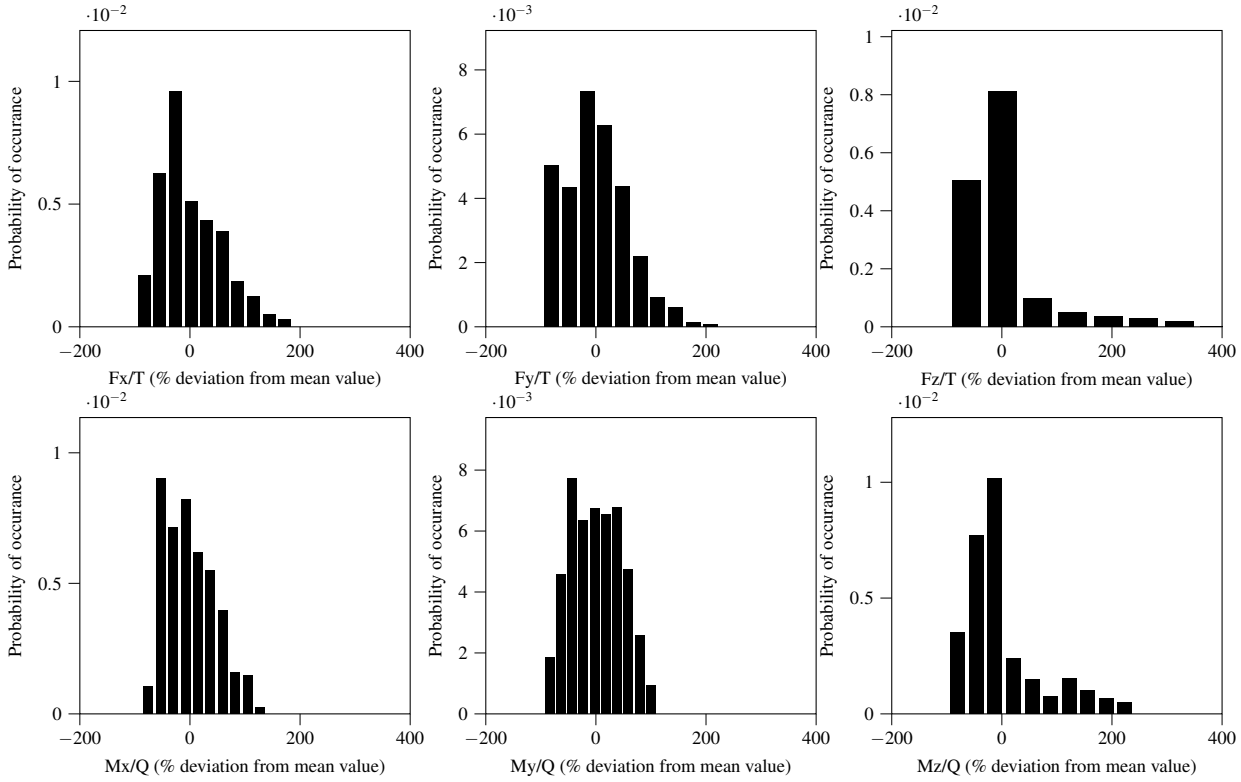

Fig. 26: Histogram of 4/rev vibratory hubforces and moments in forward flight (fiber orientation uncertainty analysis)